

CASE REPORT

Open Access



Pathologic and genomic characteristics of myoepithelioma-like tumor of the vulvar region: three case reports

Xinyu Chen^{1,2}, Qingming Jiang^{1,2}, Jue Xiao^{1,2}, Mingqiong Zhang³ and Lili Shen^{1,2*}

Abstract

Background Myoepithelioma-like tumor of the vulvar region (MELTVR) is a rare type of soft tissue mesenchymal tumor. While MELTVR exhibits histological characteristics similar to soft tissue myoepithelial tumors, its immunohistochemical and genetic features differ significantly. To date, no comprehensive genomic analysis of this tumor has been conducted.

Case presentation We present the clinicopathological features, imaging characteristics, and immunophenotypes of three patients with MELTVR, along with their genomic characterization through high-throughput sequencing. Immunohistochemical analysis revealed that these tumors were negative for SMARCB1, S-100, CD34, CD31, SMA, Desmin, and Keratin. The Ki-67 proliferation index for tumor cells ranged from 10 to 35%. Genomic analyses showed copy number deletions in the *SMARCB1* gene in all three patients. The tumor mutational burden was relatively low, ranging from 1.35 to 4.33. Additionally, two tumors exhibited fusion mutations involving *PPP6R3::FHDC1* and *MYH9::MYH6*, while no fusions involving *EWSR1*, *NR4A3*, or *FUS* were detected.

Conclusions This study reports the first comprehensive genomic analysis of three patients with MELTVR, potentially identifying therapeutic targets for this rare tumor.

Keywords Myoepithelioma-like tumor of the vulvar region (MELTVR), SMARCB1, Genomic characteristics, *PPP6R3::FHDC1*, *MYH9::MYH6*

Background

Myoepithelioma-like tumor of the vulvar region (MELTVR) is a rare soft tissue tumor derived from mesenchymal cells in the vulvar region of women [1, 2]. In 2015, Yoshida et al. reported nine patients of myoepithelioma-like tumors occurring in the vulva accompanied by a loss of SMARCB1 expression and named these tumors MELTVR [2]. To date, approximately 20 patients of MELTVR have been reported in the English literature [3]. The age at diagnosis ranges from 24 to 70 years, with a mean age of 44 years [3]. Generally, the tumor exhibits well-defined borders and a lobulated, solid-cut surface with colors varying from yellow-white to brown. The cut

*Correspondence:

Lili Shen
blkshen@cqu.edu.cn

¹Department of Pathology, Chongqing University Cancer Hospital, Chongqing 400030, P.R. China

²Chongqing Key Laboratory for Intelligent Oncology in Breast Cancer (ICQBC), Chongqing University Cancer Hospital, Chongqing 400030, P.R. China

³Department of Ultrasound, Chongqing University Cancer Hospital, Chongqing 400030, P.R. China



© The Author(s) 2025. **Open Access** This article is licensed under a Creative Commons Attribution-NonCommercial-NoDerivatives 4.0 International License, which permits any non-commercial use, sharing, distribution and reproduction in any medium or format, as long as you give appropriate credit to the original author(s) and the source, provide a link to the Creative Commons licence, and indicate if you modified the licensed material. You do not have permission under this licence to share adapted material derived from this article or parts of it. The images or other third party material in this article are included in the article's Creative Commons licence, unless indicated otherwise in a credit line to the material. If material is not included in the article's Creative Commons licence and your intended use is not permitted by statutory regulation or exceeds the permitted use, you will need to obtain permission directly from the copyright holder. To view a copy of this licence, visit <http://creativecommons.org/licenses/by-nc-nd/4.0/>.

surface appears gelatinous and glossy in some patients. At low magnification, the tumor displays clear boundaries, with multiple nodular formations separated by areas of transparent degenerative fibrous tissue. In some patients, fibrous pseudocapsules are observed, accompanied by evidence of tumor infiltration beyond the capsule [2, 4]. The tumor comprises myxoid and non-myxoid areas with varying cellularity [2, 3]. Myxoid areas contain spindle or epithelioid cells in loose reticular patterns peripherally and solid sheets centrally. Non-myxoid areas display diffuse sheets of epithelioid cells or interlacing fascicles of spindle cells. Notably, these histological features closely resemble those found in soft tissue myoepitheliomas.

Due to the clinical rarity of this condition and the lack of distinctive histological features, the misdiagnosis rate is relatively high. Its diagnosis requires a combination of immunophenotypic and molecular characteristics. MELTVR typically shows positivity for SMA, MUC1, and ER. In contrast, Keratin, Calponin, Desmin, Myogenin, S-100, glial fibrillary acidic protein (GFAP), and CD34 proteins consistently test negative. The most distinguishing features of MELTVR include the absence of SMARCB1 protein expression and *EWSR1* gene rearrangement [2, 5, 6]. Conversely, in soft tissue myoepitheliomas, approximately 50% of patients exhibit *EWSR1* gene rearrangement, while only about 10% show SMARCB1 deficiency [7, 8].

While several case reports have documented characteristic genetic alterations in MELTVR, a comprehensive genomic profile of this entity has yet to be reported. In this study, we conducted whole-exome sequencing on three patients of MELTVR, analyzing their clinicopathological features, immunophenotype, and genomic characteristics.

Case presentation

Three patients with MELTVR were collected from the Department of Pathology, Chongqing University Cancer Hospital. All tumors were located in the vulva and showed an absence of SMARCB1 expression. The tumor cells exhibited a short spindle or epithelial-like morphology, accompanied by varying degrees of a mucinous background. The tumor cells were positive for MUC1, ER, and focally positive for calponin and SMA, but negative for Keratin, CD34, and S-100. Two senior pathologists independently reviewed these patient cases.

Case 1

A 45-year-old woman accidentally discovered a lump in the mons pubis and sought medical attention at our hospital in 2016. Ultrasonography revealed a 7 mm × 17 mm hypoechoic nodule in the subcutaneous tissue of the mons pubis, characterized by clear boundaries, regular morphology, encapsulation, and posterior acoustic

enhancement. An abnormal echo in the subcutaneous soft tissue suggested enlarged lymph nodes or cysts with an inflammatory reaction (Fig. 1A). Grossly, the tumor measured approximately 15 mm × 10 mm × 10 mm and appeared gray-white with a soft, solid texture. Microscopically, the tumor boundary was clearly defined at low magnification and was encapsulated by a pseudofibrous capsule (Fig. 1B). At high magnification, the tumor displayed two distinct morphologies: one type consisted of either epithelioid or short spindle-shaped tumor cells with eosinophilic cytoplasm, uniform-sized nuclei, and eccentrically located nucleoli, situated within a stroma characterized by mucoid degeneration or loose edema (Fig. 1C, D). The second pattern involved short spindle-shaped tumor cells exhibiting bundled growth within a non-mucinous background (Fig. 1E, F). Notably, the mucoid areas comprised approximately 80% of the entire tumor volume. A mitotic figure was observed at a rate of one per 10 high-power fields (HPFs).

Immunohistochemical staining showed that the tumor cells were positive for MUC1 (Fig. 1G), vimentin, estrogen receptor (ER, Fig. 1H), progesterone receptor (PR), Calponin (Fig. 1I), and focally positive for SMA, but negative for Keratin (Fig. 1J), S-100 (Fig. 1K), Desmin and CD34. In addition, the tumor cells demonstrated a loss of SMARCB1 expression (Fig. 1L). The Ki-67 proliferation index was approximately 10%. Given the histological morphology of soft tissue myoepithelioma, which shows striated muscle-like cells with cytoplasm displacement within a mucinous matrix, and co-expresses Keratin and S100, soft tissue myoepithelioma was ruled out. Our case demonstrated an absence of expression of S-100, CD34, Desmin, and Keratin, with varying degrees of MUC1, calponin, and SMA expression. Meanwhile, the case exhibited diffuse expression of ER and a lack of SMARCB1 protein expression, leading to a diagnosis of MELTVR. Following tumor resection, the patient was followed for 89 months, with no recurrence or metastasis observed.

Case 2

A 35-year-old woman discovered a labium majus mass four months prior and sought treatment at our hospital in 2021. Ultrasound demonstrated a 28 mm × 41 mm hypoechoic nodule in the right labium majus, presenting as a micro-lobulated solid mass with an irregular pseudocapsule and clear boundaries. Internal cord-like slightly hyperechoic areas and microcystic anechoic regions were observed, with posterior acoustic enhancement. Color Doppler flow imaging showed abundant short rod-like and strip-like blood flow signals, predominantly peripheral.

Magnetic resonance imaging (MRI) showed an abnormal mass in the right vulvar region. The mass displayed heterogeneous signal intensity, being isointense on

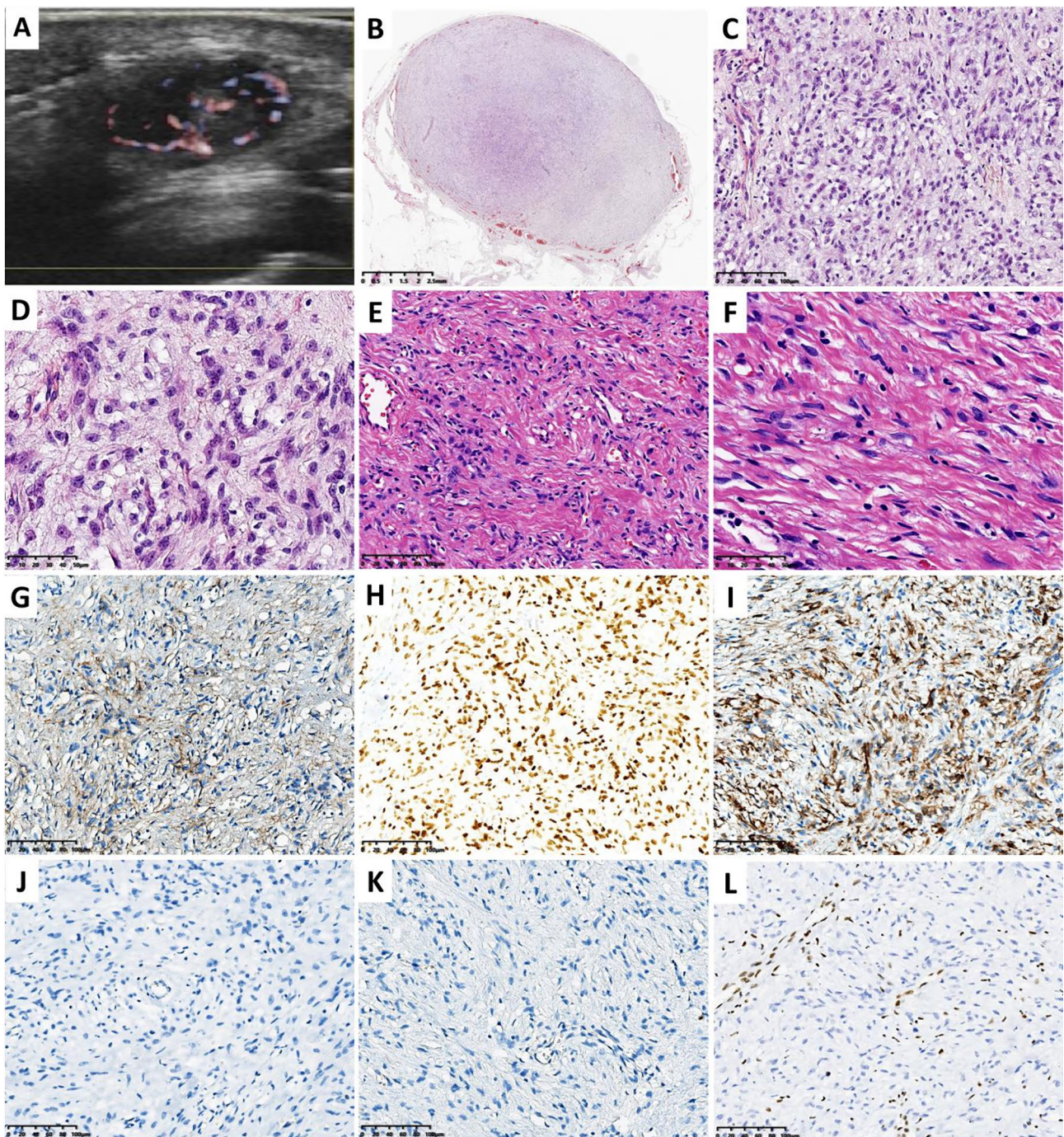


Fig. 1 Ultrasound imaging reveals a solid, hypoechoic mass with clear boundaries, exhibiting an unevenly thickened pseudocapsule at the margins (A). Tumor is focally encased by fibrous pseudocapsules (B). In myxoid areas, tumor cells exhibit either an epithelioid or spindle-shaped morphology, proliferating in a loosely cohesive reticular or clustered arrangement (C, D). In non-myxoid areas, spindle-shaped tumor cells exhibit bundled growth pattern, forming sheets (E, F). The tumor cells demonstrate focal positivity for MUC1 (G), as well as diffuse positivity for ER (H) and Calponin (I). In contrast, the tumor cells are negative for Keratin (J) and S-100 (K). SMARCB1 expression is completely absent in all tumor cells (L, vascular reactivity used as an internal positive control)

T1-weighted imaging (T1WI) and slightly hyperintense on T2-weighted imaging (T2WI) (Fig. 2A). It contained multiple focal areas of higher signal intensity, restricted diffusion on diffusion-weighted imaging (DWI), and

measured approximately 40 mm × 38 mm at its largest dimension. Additionally, the lesion exhibited persistent heterogeneous enhancement, suggesting a hypervascular neoplastic lesion in the right vulvar region.

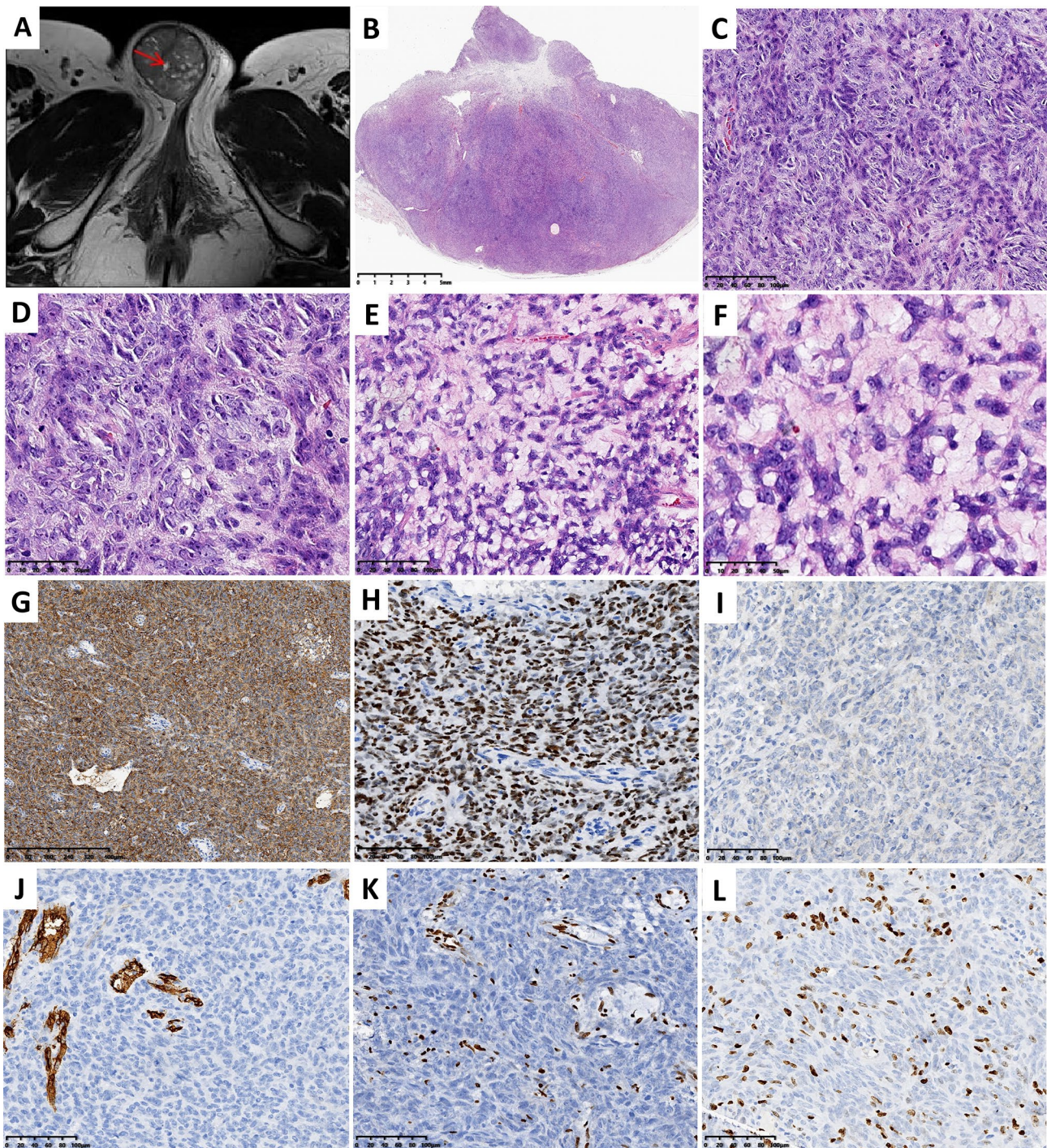


Fig. 2 T2-weighted imaging (T2W1) displays slightly hyperintense signals within the mass, with multiple punctate and patchy areas of increased signal intensity observed (red arrow, **A**). Tumor is focally encased by fibrous pseudocapsules (**B**). In non-myxoid areas, tumor cells exhibit either an epithelial-like or spindle-shaped morphology, with biphasic cytoplasm, moderate cellular pleomorphism, prominent nucleoli, and a diffuse, sheet-like arrangement (**C**, **D**). In myxoid areas, epithelioid or spindle-shaped tumor cells proliferate in a loosely cohesive reticular or clustered manner (**E**, **F**). The tumor cells show diffuse positivity for MUC1 (**G**) and ER (**H**) but are negative for Keratin (**I**) and CD34 (**J**). SMARCB1 expression remains absent in all tumor cells (**K**, vascular reactivity used as an internal positive control). The Ki-67 proliferation index is approximately 15% (**L**)

Macroscopically, the tumor measured approximately 55 mm × 50 mm × 40 mm and had a gray-white appearance with a soft solid texture. Microscopically, histological images revealed the tumor was surrounded by a fibrous pseudocapsule with clear boundaries at low magnification (Fig. 2B). At high magnification, the tumor cells exhibited some degree of atypia. The histological morphology displayed two distinct cellular patterns. One pattern was characterized by tumor cells exhibiting either an epithelial-like or spindle-shaped morphology, with biphasic cytoplasm, moderate cellular pleomorphism, prominent nucleoli, and a diffuse, sheet-like arrangement (Fig. 2C, D). Another pattern showed epithelial-like tumor cells distributed sporadically in the mucous matrix (Fig. 2E, F). Notably, the mucoid areas comprised approximately 10% of the entire tumor volume, with a mitotic figure observed at a rate of 7 per 10 HPFs.

Immunohistochemical staining showed that the tumor cells were positive for MUC1 (Fig. 2G), ER (Fig. 2H), PR, and vimentin, with focal positivity for SMA. However, the tumor cells tested negative for Keratin (Fig. 2I), S-100, Desmin, and CD34 (Fig. 2J). In addition, the tumor cells demonstrated a loss of SMARCB1 expression (Fig. 2K). The Ki-67 proliferation index was approximately 15% (Fig. 2L). The tumor had clear boundaries and was not accompanied by necrosis. Although the tumor cells exhibited an epithelial-like morphology, they did not express Keratin, S-100, CD34, or SMARCB1. This morphology, along with the immunohistochemical profile, effectively ruled out the possibility of epithelial sarcoma, leading to a diagnosis of MELTVR. Following tumor resection, the patient underwent a vulvar wide excision and was followed for 35 months, with no recurrence or metastasis observed.

Case 3

A 45-year-old woman accidentally discovered a lump in the mons pubis. An ultrasound examination revealed a hypoechoic nodule measuring 21 mm × 6 mm within the adipose layer of the right mons pubis. The patient underwent tumor resection at an outside hospital and later sought a pathology consultation at our facility.

Macroscopically, the surgical specimen consisted of multiple fragments, totaling approximately 80 mm × 80 mm × 25 mm. The specimen appeared pale brown with a soft, solid texture. Microscopically, the tumor tissue was fragmented, making it challenging to assess its boundaries at low magnification (Fig. 3A). At high magnification, the tumor cells exhibited varying degrees of atypia. The histological morphology resembled that of Case 2 and was characterized by two distinct cellular patterns. One pattern featured tumor cells with epithelial-like or spindle-shaped morphology, biphasic cytoplasm, moderate cellular pleomorphism, prominent nucleoli,

and a diffuse arrangement of tumor cells in a sheet-like pattern (Fig. 3B-D). Another pattern showed scattered arrangements of short spindle-shaped or epithelial-like tumor cells in a mucinous background (Fig. 3E, F). The mucoid areas comprised approximately 10% of the entire slide, with a mitotic figure observed at a rate of 12 per 10 HPFs.

Immunohistochemical staining revealed that the tumor cells were focally positive for MUC1 (Fig. 3G) and diffusely positive for vimentin and ER (Fig. 3H). The cells were negative for Keratin (Fig. 3I), CD34 (Fig. 3J), P63, and SMA. In addition, the tumor cells demonstrated a loss of SMARCB1 expression (Fig. 3K). The Ki-67 proliferation index was approximately 20% (Fig. 3L). The tumor cells displayed an epithelial-like morphology and did not express Keratin, S-100, or SMARCB1, effectively ruling out the possibility of soft tissue myoepithelioma and epithelial sarcoma. Consequently, the diagnosis was confirmed as MELTVR. Following tumor resection, the patient was followed for 8 months, with no recurrence or metastasis observed.

Genomic characteristics

Whole-exome sequencing (WES) was performed on DNA isolated from tumor tissue for all three patients. Additionally, peripheral blood was collected from Patient 2 (C122201) to identify germline mutations. Due to severe RNA degradation in Patient 1 (C122202), gene fusion analysis based on RNA sequencing was only performed for Patients 2 (C122201) and 3 (C122203).

WES revealed that missense mutations were the most prevalent type of mutation observed, with the tumor mutational burden (TMB) in the three patients being relatively low (ranging from 1.35 to 4.33). Copy number variation (CNV) analysis indicated that gene deletions were the predominant type, while gene amplifications were rare (Fig. 4A). All three patients exhibited deletions in the *SMARCB1* gene (Fig. 4B-D). Additionally, RNA sequencing facilitated the identification of two novel fusions: *PPP6R3::FHDC1* and *MYH9::MYH6* (Fig. 4E); however, no fusions involving genes such as *EWSR1*, *NR4A3*, or *FUS* were detected.

Discussion and Conclusions

MELTVR, as a rare SMARCB1-deficient mesenchymal neoplasm of the vulvar region, exhibits distinctive immunophenotypic and genomic characteristics. The clinical and pathological features of the reported 21 patients in the English literature and our cases are summarized in Table 1. The tumor consists of mucinous and non-mucinous areas, with a distribution of cellular-rich regions [2, 4, 9–11]. The histological morphology observed in the three patients presented in this study is consistent with the descriptions reported in the literature.

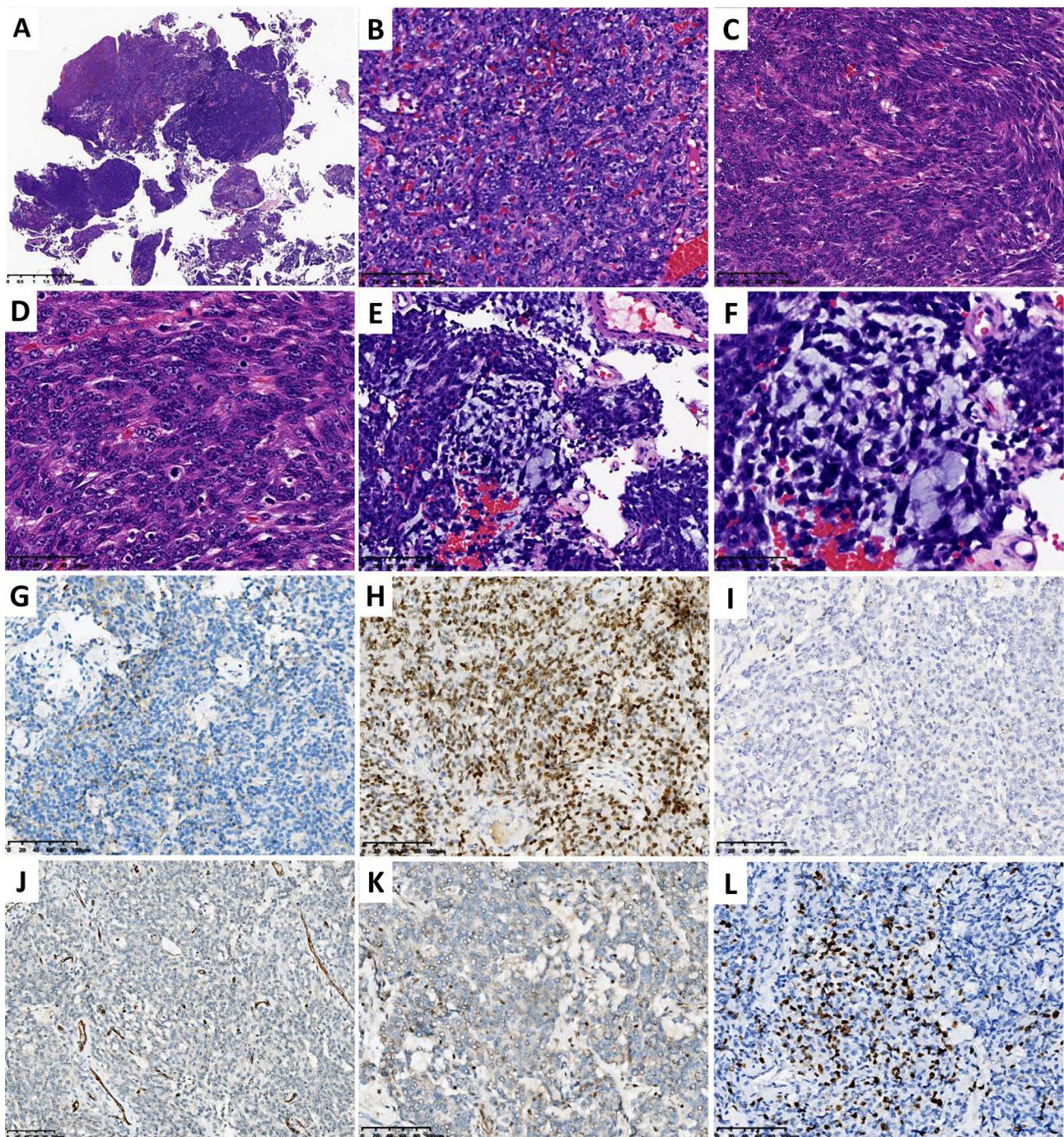


Fig. 3 The tumor tissue is fragmented (A). In non-myxoid areas, tumor cells exhibit either an epithelial-like or spindle-shaped morphology, with biphasic cytoplasm, moderate cellular pleomorphism, prominent nucleoli, and a diffuse, sheet-like arrangement (B-D). In myxoid areas, epithelioid or spindle-shaped tumor cells proliferate singly or in a loosely cohesive reticular or clustered manner (E, F). The tumor cells show focal positivity for MUC1 (G), as well as diffuse positivity for ER (H). In contrast, the tumor cells are negative for Keratin (I) and CD34 (J). SMARCB1 expression is completely absent in all tumor cells (K, vascular reactivity used as an internal positive control). The Ki-67 proliferation index is approximately 20% (L)

Immunohistochemically, the tumor cells are positive for vimentin, MUC1, ER, and PR, with ER and PR exhibiting either partial or diffuse positivity. All tumor cells also show a deficiency in SMARCB1 expression. In some patients, the tumor cells are also positive for

SMA, ERG, STAT6, CD34, Calponin, and Keratin [1–4, 9, 12], but completely negative for Desmin, Myogenin, SOX10, p63, S-100, and GFAP. All three patients presented in this study exhibited MUC1 and ER expression, with loss of SMARCB1 expression. Patients 1 and 2 also

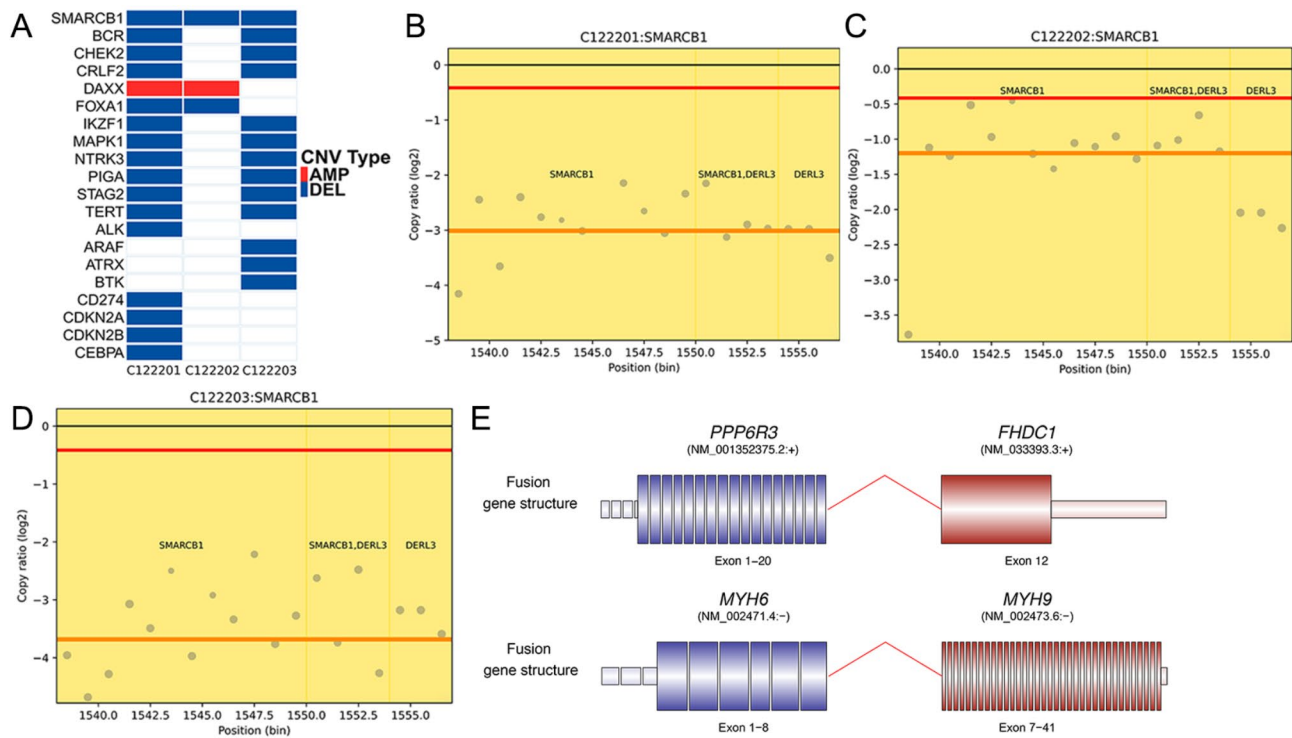


Fig. 4 Genomic characteristics of MELTVRs. Distribution of the top 20 genes with CNVs (A). Copy number distribution of the *SMARCB1* gene in patients (B-D). The red line represents the threshold, the pink line indicates the logarithmic values of copy numbers, and the points represent the bins. Schematic diagram of gene fusion (E)

Table 1 Case reports of MELTVR in english literature

Authors and year	Number of cases	Mean age(range), years	Mean tumor size (range), cm	Treatment	Molecular analysis	Recurrence	Metastases	Follow-up time, months
Yoshida et al. (2015)	9	41(24–65)	4.6(2-7.7)	Excision	Lost of INI1/ <i>SMARCB1</i>	3/9	None	1 to 172 (mean, 66), alive
Tajima et al. (2015)	1	42	1.5	Excision	Lost of INI1/ <i>SMARCB1</i>	Yes	None	5, alive
Kaku et al. (2016)	1	31	2	Excision	Lost of INI1/ <i>SMARCB1</i>	None	None	11, alive
Kojima et al. (2019)	1	70	3.6	Excision	Lost of INI1/ <i>SMARCB1</i>	None	None	12, alive
Zhang et al. (2019)	1	34	3	Excision	Lost of INI1/ <i>SMARCB1</i>	None	None	6, alive
Segawa et al. (2020)	2	38–70	3.6-4	Excision	Lost of INI1/ <i>SMARCB1</i>	None	None	3 to 12, alive
Xu et al. (2020)	1	65	5.5	Excision	Lost of INI1/ <i>SMARCB1</i>	None	None	8, alive
Lin et al. (2021)	1	49	3	Excision	Lost of INI1/ <i>SMARCB1</i>	None	None	6, alive
Liu et al. (2022)	1	43	4.2	Excision	Lost of INI1/ <i>SMARCB1</i>	None	None	8, alive
Hammer et al. (2022)	2	31–69	1.8–5.8	Excision	Lost of INI1/ <i>SMARCB1</i>	None	None	10, alive
Aminimoghaddam et al. (2023)	1	46	9	Excision	Lost of INI1/ <i>SMARCB1</i>	None	None	36, alive
Present	3	35–45	1.7-4.0	Excision	Lost of INI1/ <i>SMARCB1</i>	None	None	8 to 89, alive

demonstrated calponin expression, which is consistent with existing literature [3, 9].

Although MELTVR can be differentiated from other SMARCB1-deficient tumors through immunophenotypic and genomic analysis, our understanding of the comprehensive genomic features of MELTVR remains limited. In this report, we present, for the first time, an analysis of the genomic characteristics of three patients of MELTVR utilizing high-throughput sequencing technology. The TMB of MELTVR was relatively low. In all three patients, there was a deletion of the *SMARCB1* gene copy number. Additionally, fusion mutations involving the *PPP6R3::FHDC1* and *MYH9::MYH6* genes were identified in two of these tumors, respectively. *FHDC1* is an actin-regulating factor with scaffolding functions, associated with organ development and tumorigenesis. The *MYH9* has been shown to inhibit the migration and invasion of tumor cells in various cancers, including ovarian cancer, osteosarcoma, hepatocellular carcinoma, and malignant melanoma, exerting an anti-tumor effect [13–16]. However, the fusion mutations involving *PPP6R3::FHDC1* and *MYH9::MYH6* are exceedingly rare and have not been previously reported to date.

MELTVR should be differentiated from a spectrum of neoplasms, including soft tissue myoepithelioma, extraskeletal myxoid chondrosarcoma (EMC), epithelioid sarcoma (ES), extrarenal malignant rhabdoid tumor (E-MRT), and benign mesenchymal neoplasms with a predilection for the women genital tract (such as cellular angiofibroma, aggressive angiomyxoma, and angiofibrosarcoma).

MELTVR has a similar histological pattern to soft tissue myoepithelioma; however, their immunophenotypic and genetic profiles differ substantially. Firstly, the majority of MELTVR patients demonstrate negative Keratin expression, and all tumors lack reactivity for S-100 protein and GFAP. In contrast, 90% of myoepitheliomas express Keratin, and 85% express S-100 protein [17]. Secondly, while some myoepitheliomas may show loss of SMARCB1 protein expression, all MELTVR consistently lack SMARCB1 protein immunoreactivity [7]. Furthermore, approximately 50% of soft tissue myoepitheliomas harbor *EWSR1* gene rearrangements, whereas *EWSR1* gene rearrangements have not been identified in any MELTVR [8]. The IHC results for our three tumors demonstrated an absence of expression of S-100, CD34, CD31, SMA, Desmin, and Keratin, with varying degrees of MUC1 expression. All three tumors exhibited a lack of SMARCB1 protein expression, and the Ki-67 proliferation index ranged from 10 to 35%.

EMC usually occurs in the deep soft tissues of the limbs in middle-aged and elderly patients, with rare involvement in the superficial perineal area. Microscopically, it displays a lobulated pattern composed of tumor cells

distributed in a cord-like or mesh-like fashion within a myxoid matrix, with sparse interstitial vessels. The cytoplasm of tumor cells is deeply eosinophilic, showing fine granular or vacuolated features, and mitotic figures are rare. Expression of MUC1 and ER in EMC is uncommon, with 90% showing *NR4A3* gene rearrangement [18, 19].

ES, particularly the proximal type, can involve the vulvar region and exhibits infiltrative growth with areas of necrosis. The tumor is composed of epithelioid tumor cells with vesicular nuclei, evident atypia, prominent nucleoli, frequent mitotic figures, and pathological mitoses. ES almost always expresses Keratin, 50–70% expresses CD34, 90% exhibit SMARCB1 deficiency, and concurrent *SMARCB1* gene deletion or mutation is present [1, 7].

E-MRT predominantly affects the midline deep soft tissues of infants and children, comprising sheets of round or polygonal rhabdoid cells. The tumor cells have large nuclei with chromatin in a vacuolated pattern, prominent nucleoli, and frequent mitotic figures, and are often associated with hemorrhage and necrosis. Tumor cells express Keratin, Vimentin, MUC1, and *SALL4*, with loss of SMARCB1 protein expression, and concurrent occurrence of homozygous *SMARCB1* gene deletion or mutation [20].

The imaging manifestations of tumors are closely related to the histopathology; however, there are currently scarce imaging reports on this tumor. Patient 1 appeared as a well-defined hypoechoic mass on ultrasound, with thick and uneven linear hyperechoic lines at the margins, possibly representing the fibrous pseudocapsule of the tumor. The internal short linear hyperechoic lines corresponded to fibrous structures of varying widths, with some areas showing cystic hypoechoic regions related to tumor hemorrhage and necrosis [2, 4]. In patient 2, the tumor had indistinct borders, with fine spicules at the periphery indicative of infiltration into the surrounding fat tissue from outside the tumor capsule [2, 4]. Histologically, the tumor stroma was rich in blood vessels with elongated branching vessels, showing sclerosis in the walls of medium and small vessels, visualized on ultrasound as abundant short rod-shaped and linear blood flow signals, a feature observed in both Patient 1 and Patient 2. The Patient 1's MRI-enhanced scan showed sustained uneven enhancement. The imaging features of this disease are difficult to differentiate from vascular-rich tumors in soft tissues such as hemangiomas, vascular fibromas, and sarcomas, necessitating immunohistochemistry and genetic molecular studies for a definitive diagnosis.

In conclusion, we identified for the first time the presence of *PPP6R3::FHDC1* and *MYH9::MYH6* gene fusions in MELTVR, potentially providing therapeutic targets for the treatment of recurrent MELTVR. Although

no common mutations were found among the three patients, this study marks the first revelation of MELTVR's genomic characteristics. We aim to collect more patient data to develop a more comprehensive genomic atlas of MELTVR.

Materials

Immunohistochemistry

Immunohistochemical analysis was performed on 4- μ m FFPE tissue sections using the following antibodies and conditions: Keratin (clone: MX005, Maixin Biotech, Fuzhou, China), vimentin (clone: MX034, Maixin Biotech, Fuzhou, China), S-100 (clone: MXR034, Maixin Biotech, Fuzhou, China), MUC1 (clone: E29, Maixin Biotech, Fuzhou, China), Calponin, (clone: MX023, Maixin Biotech, Fuzhou, China), SMA (clone: MX097, Maixin Biotech, Fuzhou, China), CD34 (clone: MX123, Maixin Biotech, Fuzhou, China), estrogen receptor (ER, clone: SP1, Maixin Biotech, Fuzhou, China), progesterone receptor (PR, clone SP2, Maixin Biotech, Fuzhou, China), SMARCB1 (clone MRQ27, Maixin Biotech, Fuzhou, China), Ki-67 (clone MXR002, Maixin Biotech, Fuzhou, China), Desmin (clone MX046, Maixin Biotech, Fuzhou, China), and P63 (clone MX013, Maixin Biotech, Fuzhou, China). The EnVision Plus detection system (Dako, Glostrup, Denmark) was used for all antibodies. Standard procedures and antigen retrieval protocols were followed. Appropriate positive and negative controls were included throughout.

Next generation sequencing

Simultaneous extraction of RNA and DNA from tissue samples, and gDNA from peripheral blood, was performed using the Nucleic Acid Isolation Kit (Novogene, Tianjin, China). The concentration of DNA and RNA was tested with a Qubit 4.0 Fluorometer (Life Technologies, CA, USA). In addition, DNA and RNA integrity were tested in the Bioanalyzer 2100 system (Agilent Technologies, CA, USA). DNA and RNA library hybridization capture was conducted using the Novogene WES Plus Panel and RNA Fusion Panel, respectively (Novogene, Tianjin, China). All libraries were sequenced on the NovaSeq X Plus platform (Illumina, CA, USA). For data analysis, BWA and STAR were used to align DNA and RNA sequence data to the reference genome (hg19), respectively. VarScan, Samtools, and GATK were employed to call DNA SNVs/Indels, while Delly was used for DNA fusion detection. STAR-Fusion was utilized for RNA fusion calling.

Abbreviations

CNV	Copy number variation
EMC	Extraskeletal myxoid chondrosarcoma
E-MRT	Extrarenal malignant rhabdoid tumor
ES	Epithelioid sarcoma

ER	Estrogen receptor
FFPE	Formalin-fixed paraffin-embedded
HPF	High-power fields
IHC	Immunohistochemical
MELTVR	Myoepithelioma-like tumor of the vulvar region
PR	Progesterone receptor
TMB	Tumor mutation burden
WES	Whole Exome Sequencing

Author contributions

LS conceived the study and reviewed the manuscript. XC performed data collection and analysis and drafted the manuscript. QJ and JX contributed to data collection. MZ contributed to the analysis of ultrasound imaging data. All authors read and approved the final manuscript.

Funding

None.

Data availability

All data generated or analyzed during this study are included in this article. Further inquiries should be directed to the corresponding author.

Declarations

Ethics approval and consent to participate

This study was reviewed and approved by the Ethics Committee of Chongqing University Cancer Hospital (CZLS0224118-A).

Consent for publication

Written informed consent was provided by all participants.

Competing interests

The authors declare no competing interests.

Received: 13 February 2025 / Accepted: 23 March 2025

Published online: 05 April 2025

References

1. Folpe AL, Schoolmeester JK, McCluggage WG, Sullivan LM, Castagna K, Ahrens WA, et al. SMARCB1-deficient vulvar neoplasms: A clinicopathologic, immunohistochemical, and molecular genetic study of 14 cases. *Am J Surg Pathol*. 2015;39(6):836–49.
2. Yoshida A, Yoshida H, Yoshida M, Mori T, Kobayashi E, Tanzawa Y, et al. Myoepithelioma-like tumors of the vulvar region: A distinctive group of SMARCB1-deficient neoplasms. *Am J Surg Pathol*. 2015;39(8):1102–13.
3. Liu X, Chen L, Zhou Q, Liu J, Hu Y. Myoepithelioma-like tumors of the vulvar region: A case report and review of the literature. *J Obstet Gynaecol Res*. 2022;48(7):2015–20.
4. Kaku Y, Goto K, Kabashima K. Myoepithelioma-like tumor of the vulvar region presenting as a nonmyxoid Spindle-Cell neoplasm: A potential histologic mimicker of solitary fibrous tumor. *Am J Dermatopathol*. 2016;38(7):e87–9.
5. Jo VY, Antonescu CR, Zhang L, Dal Cin P, Hornick JL, Fletcher CD. Cutaneous syncytial myoepithelioma: clinicopathologic characterization in a series of 38 cases. *Am J Surg Pathol*. 2013;37(5):710–8.
6. Kurzawa P, Kattapuram S, Hornicek FJ, Antonescu CR, Rosenberg AE, Nielsen GP. Primary myoepithelioma of bone: a report of 8 cases. *Am J Surg Pathol*. 2013;37(7):960–8.
7. Hornick JL, Dal Cin P, Fletcher CD. Loss of INI1 expression is characteristic of both conventional and proximal-type epithelioid sarcoma. *Am J Surg Pathol*. 2009;33(4):542–50.
8. Antonescu CR, Zhang L, Chang NE, Pawel BR, Travis W, Katani N, et al. EWSR1-POU5F1 fusion in soft tissue myoepithelial tumors. A molecular analysis of sixty-six cases, including soft tissue, bone, and visceral lesions, showing common involvement of the EWSR1 gene. *Genes Chromosomes Cancer*. 2010;49(12):1114–24.
9. Xu Y, Gao H, Gao JL. Myoepithelioma-like tumor of the vulvar region: a case report in China and review of the literature. *Diagn Pathol*. 2020;15(1):3.
10. Zhang HZ, Wang SY. Myoepithelioma-like tumour of the vulvar region. *Pathology*. 2019;51(6):665–8.

11. Kojima Y, Tanabe M, Kato I, Motoi T, Kimura M, Sawazumi T, et al. Myoepithelioma-like tumor of the vulvar region showing infiltrative growth and harboring only a few Estrogen receptor-positive cells: A case report. *Pathol Int.* 2019;69(3):172–6.
12. Tajima S, Takahasi Y, Hikoaki M, Goto R. A SMARCB1-deficient vulvar neoplasm with prominent myxoid stroma: report of a case showing ERG and FLI1 expression. *Int J Clin Exp Pathol.* 2015;8(6):7526–32.
13. Wang S, Wang Y, Lu J, Wang J. LncRNA LINC00665 promotes ovarian cancer cell proliferation and inhibits apoptosis via targeting miR-181a-5p/FHDC. *Appl Biochem Biotechnol.* 2022;194(9):3819–32.
14. Qu Y, Lu J, Mei W, Jia Y, Bian C, Ding Y, et al. Prognostic biomarkers of pancreatic cancer identified based on a competing endogenous RNA regulatory network. *Translational cancer Res.* 2022;11(11):4019–36.
15. Copeland SJ, McRae A, Guarguaglini G, Trinkle-Mulcahy L, Copeland JW. Actin-dependent regulation of cilia length by the inverted Formin FHDC1. *Mol Biol Cell.* 2018;29(13):1611–27.
16. Copeland J. Actin-based regulation of ciliogenesis— The long and the short of it. *Semin Cell Dev Biol.* 2020;102:132–8.
17. Hornick JL, Fletcher CD. Myoepithelial tumors of soft tissue: a clinicopathologic and immunohistochemical study of 101 cases with evaluation of prognostic parameters. *Am J Surg Pathol.* 2003;27(9):1183–96.
18. Oliveira AM, Sebo TJ, McGrory JE, Gaffey TA, Rock MG, Nascimento AG. Extraskeletal myxoid chondrosarcoma: a clinicopathologic, immunohistochemical, and ploidy analysis of 23 cases. *Mod Pathology: Official J United States Can Acad Pathol Inc.* 2000;13(8):900–8.
19. Okamoto S, Hisaoka M, Ishida T, Imamura T, Kanda H, Shimajiri S, et al. Extraskeletal myxoid chondrosarcoma: a clinicopathologic, immunohistochemical, and molecular analysis of 18 cases. *Hum Pathol.* 2001;32(10):1116–24.
20. Wang H, Ma Y, Li J, Zhang D, Wu B, Fang C, et al. Extrarenal malignant rhabdoid tumor of childhood: a clinicopathologic analysis of 8 cases. *Zhonghua Bing Li Xue Za zhi = Chinese J Pathol.* 2014;43(12):805–8.

Publisher's note

Springer Nature remains neutral with regard to jurisdictional claims in published maps and institutional affiliations.